Competitive metastable phase in low-temperature epitaxy of $CoSi_2$/Si(111)

S. Goncalves-Conto, U. Schärer, E. Müller, and H. von Känel
Laboratorium für Festkörperphysik, ETH Zürich, CH-8093 Zürich, Switzerland

L. Miglio and F. Tavazza
Instituto Nazionale di Fisica della Materia and Dipartimento di Fisica dell'Università di Milano, via Celoria 16, I-20133 Milano, Italy
(Received 30 September 1996)

We analyzed the structural, elastic, and electric properties of $CoSi_2$ films grown by stoichiometric codeposition onto Si(111) substrates. Films growing epitaxially at room temperature onto an ultrathin template, and films nucleating from the amorphous phase after a mild anneal, were considered. Both were found to crystallize predominantly with a CsCl-derived defect structure with random occupation of the metal sites. The kinetics of the phase transition to the stable bulk phase with the fluorite structure appears to be different for the two growth procedures. After annealing to 600 °C, grains with the CsCl defect structure were found to be present mainly in films grown on a template. This also explains the poorer electrical properties of these films. A microscopic model which explains the easy formation and the persistence of the CsCl-defected phase is derived on the basis of tight-binding molecular dynamics. [S0163-1829(97)00507-9]

I. INTRODUCTION

In the past few years, the synthesis of $CoSi_2$ films on silicon has been the subject of numerous studies. The stable phase of $CoSi_2$ has a cubic CaF_2 structure with $a=5.36$ Å, so that its lattice mismatch with respect to silicon is small at room temperature (-1.2%). Its electrical properties, such as a low resistivity ($\rho_{300\ K}=16\ \mu\Omega$ cm and $\rho_{4.2\ K}=2.5\ \mu\Omega$ cm), and the metallic behavior still present in films as thin as 10 Å,[1] as well as the rather high thermal stability, make $CoSi_2$ a promising candidate for microelectronic and optoelectronic applications in Si technology.[2–5] Since any imperfection may spoil these electric properties, controlling the quality of the films is very important, and the understanding of their microstructure as a function of the growth parameters is required.

One of the first techniques used to grow $CoSi_2$ on Si(111) was solid-phase epitaxy, consisting of room-temperature deposition of cobalt followed by reactive annealing up to 650 °C,[6] or by molecular-beam epitaxy (MBE) carried out at equally high substrate temperatures.[7] This resulted in films with a poor morphology, and for this reason was replaced by more elaborate techniques. In particular, smooth surfaces without pinholes can be achieved by sequential deposition of Co and Si,[8,9] or by stoichiometric coevaporation onto cold substrates, followed by annealing in order to avoid long diffusion paths.[10–12] Pinholes could be prevented from forming by these methods, in contrast to dislocations. In order to grow films with a low dislocation density, Tung and Schrey[13] developed a ''template technique.'' An ultrathin (typically 10 Å) $CoSi_2$ layer, the template, is grown first, and subsequently the silicide film can be synthesized at room temperature by MBE. The template can be formed either by stoichiometric codeposition[14] or by deposition of a small amount of pure Co,[13] with identical results after the annealing. It was also demonstrated that the defect structure in the films depends strongly on the quality of the $CoSi_2$ template, and that the remaining interfacial dislocations are associated with steps at the Si/silicide interface.[13]

One other source of electric quality deterioration may stem from the formation of metastable phases. On Si(100) substrates, the sporadic appearance of a highly metastable phase has been reported, when reacting Co/Ti bilayers with Si.[15] It is based on a diamond Si sublattice with Co interstitials, called the *adamantane* structure. On Si(111), another metastable $CoSi_2$ phase is actually formed in the previously described ''template technique,'' rather than the bulk phase with the CaF_2 structure, as originally assumed.[16,17] The crystal structure of this phase may be derived from the CsCl structure in which the monosilicides of Fe and Co were shown to be epitaxially stable when grown by MBE at low substrate temperatures.[18,19] In the case of stoichiometric disilicides, 50% of vacancies are statistically distributed on the cation sites.[20,21]

In this paper, we show that the defect CsCl phase is present in $CoSi_2$ films, grown with or without the use of templates, provided that they are grown at sufficiently low substrate temperatures. In the following this phase will be designated with $Co_{0.5}Si$ in order to distinguish it from $CoSi_2$ with the fluorite structure. In Sec. II the details of sample fabrication and experimental techniques are given. After the presentation of the structural characteristics (Sec. III), the elastic properties of this phase are shown in Sec. IV. The thermal stability of the phase is studied by post-growth annealing (Sec. V), and the results of total-energy calculations and molecular-dynamics simulations provide a kinetic explanation of the experimental findings (Sec. VI). The correlation between the microstructure and electrical properties is finally presented in Sec. VII.

II. EXPERIMENT

The silicide films were grown by electron beam evaporation of Si and Co in a commercial MBE system on 3-in. Si(111) substrates (*n* doped, 25–50 Ω cm). Film thicknesses ranged between ~30 and 1000 Å. The substrate preparation procedure is described in detail in Ref. 14. All depositions

 © 1997 The American Physical Society

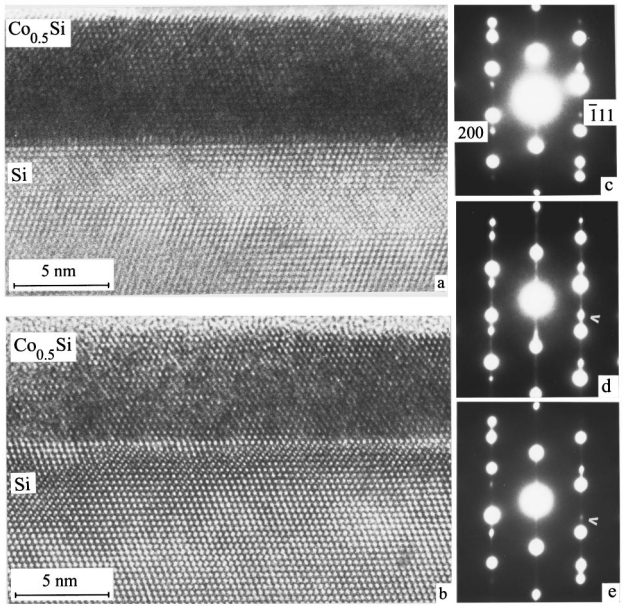

FIG. 1. High-resolution images and the corresponding diffraction pattern of two $Co_{0.5}Si$ films of 60 Å grown on the same substrate with template (a) and (c) and without template (b) and (e). The diffraction spots of the silicides are indexed with respect to the cubic Si unit cell. (d) Diffraction pattern of $(CaF_2)CoSi_2$.

started on clean 7×7-reconstructed Si(111) surfaces with parallel monolayer steps due to unintentional wafer misorientation of less than 0.10°. The films were grown in two ways.

(i) At first a 10-Å-thick $CoSi_2$ template was formed by stoichiometric codeposition of Co and Si onto the substrate kept at room temperature (RT). The template was then annealed at 420 °C for 5 min, and cooled down to RT. Thicker films were grown onto this template by MBE with typical deposition rates of 1 Å/s, and finally capped with a 40-Å-thick amorphous Si layer.

(ii) For the sake of comparison, some films were grown both with and without the template on the same substrate, by masking half of the substrate during template formation. They were then crystallized also in the template-free region by annealing to 200–210 °C for a few minutes, and again capped with *a*-Si.

Before capping, the films were characterized *in situ* by reflection high-energy electron diffraction (RHEED). *Ex situ* characterizations were carried out by x-ray diffraction (XRD) on a computer-controlled diffractometer using Cu-$K\alpha_1$ radiation, by high-resolution transmission electron microscopy (HRTEM), and by Brillouin spectroscopy measurements (BS). Electric transport measurements were carried out in a liquid-helium cryostat, on specimens patterned in the form of a standard five-leg bridge, prepared by photolithography and wet chemical etching. The electrical resistivities were measured between 4.2 and 300 K, and the Hall effect at 4.2 K in magnetic fields up to 5 T.

III. STRUCTURAL CHARACTERIZATION

A. TEM measurements

Figure 1 shows high-resolution images and the corresponding diffraction patterns of a 60-Å-thick $Co_{0.5}Si$ film grown onto a 10-Å-thick template with the CaF_2 structure [Figs. 1(a) and 1(c)], and without a template [Figs. 1(b) and 1(e)], and annealed at 210 °C. Similar findings have been found in both cases:

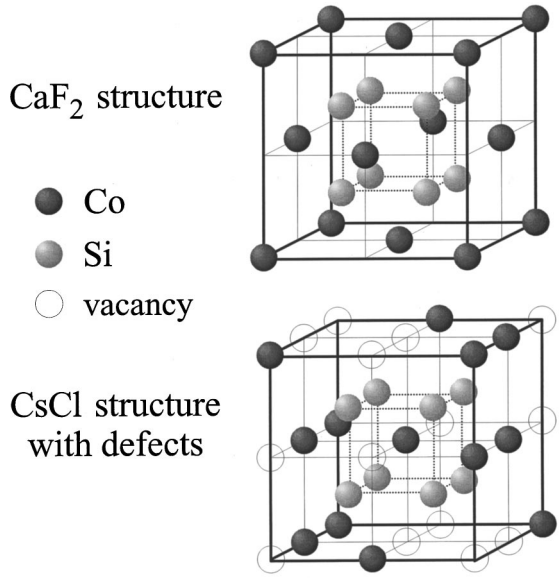

FIG. 2. Sketch of the unit cell of $CoSi_2$ with the CaF_2 structure (a), and the stoichiometric $Co_{0.5}Si$ with the CsCl structure (b).

(i) The orientation of the epitaxial film is of type *B*, i.e., rotated by 180° around the substrate normal.

(ii) When the diffraction spots are indexed according to a cubic cell with the lattice parameter a_{Si} of Si, all (hkl) reflections with odd indices are very weak. The arrow points to the position of the nearly missing (111) spot [Figs. 1(c) and 1(e)]. This is consistent with the CsCl structure and a lattice parameter a_0 of the film close to $a_{Si}/2$.[18] By contrast, these spots are much stronger in the CaF_2 structure [Fig. 1(d)].

On the HRTEM images, only faint indications of the presence of a CsCl structure can be recognized. By computer simulations of the image contrast it could be shown that the typical CsCl-image contrast only appears if more than 80% of the Co atoms are disordered. If more than 20% of the Co has fluorite structure, the image contrast is already indistinguishable from that of pure fluorite. For the simulations a continuous change from CaF_2 to CsCl structure, and a statistical distribution of the two phases, were assumed. The details of these simulations will be published elsewhere.

According to the simulations, the observation of a fluoritelike HRTEM image contrast is not in contradiction with the diffraction patterns, indicating the dominating presence of $Co_{0.5}Si$ with CsCl structure. From the image contrast and the corresponding computer simulations, the presence of an *adamantane* structure can clearly be excluded. The unit cells of $CoSi_2$ with a CaF_2 structure, and with a CsCl-defect structure with random vacancies in the cation sublattice, are shown for comparison in Fig. 2.

B. XRD measurements

The crystal structure, the lattice constant, and the strain of the films were determined by XRD measurements. If elastic strains are present in an epitaxial layer, the lattice constant a_0

of the relaxed structure cannot be measured directly. The elastic distortion leads to a symmetry lowing from cubic to trigonal due to the Poisson effect. The resulting planar strain is given by

$$\varepsilon_{\parallel}=\frac{(a_{\parallel}-a_0)}{a_0}, \tag{1}$$

and the associated perpendicular strain is

$$\varepsilon_{\perp}=\frac{(a_{\perp}-a_0)}{a_0}. \tag{2}$$

Here $a_{\parallel}$ and $a_{\perp}$ are the in-plane and perpendicular lattice parameters of the trigonal structure, respectively. For elastically isotropic materials the trigonal strain $\varepsilon_t=\varepsilon_{\parallel}-\varepsilon_{\perp}$ depends on $\varepsilon_{\parallel}$ in the following way:[22]

$$\varepsilon_t=\frac{(a_{\parallel}-a_{\perp})}{a_0}=\left(\frac{1+\nu}{1-\nu}\right)\varepsilon_{\parallel}, \tag{3}$$

where ν is the Poisson ratio. In Sec. IV it will be shown that the assumption of isotropy is indeed justified for the $Co_{0.5}Si$ phase.

Because XRD Bragg peaks of thin layers are both weak and broad, as predicted by dynamical diffraction theory,[23] no detectable symmetrical diffractions were found. Theoretical calculations[24] of peak intensities show that asymmetrical reflections are about ten times as large as symmetrical reflections. For this reason only the asymmetrical {440}, {422}, and {331} reflections were measured. The former two are sufficient to determine $a_{\perp}$ and $a_{\parallel}$ independently.[24] In agreement with the TEM measurements, diffraction peaks with odd order indices were found to be absent for annealing temperatures below ~210 °C, i.e., the films crystallize predominantly with the CsCl structure. Films grown onto an ultrathin $CoSi_2$ template with the CaF_2 structure formed an exception in that the {331} diffraction peaks were nevertheless observed. The absolute intensity of this reflection was, however, independent of the film thickness, and must hence be attributed to diffraction from the template.

According to Eqs. (1) and (3), the lattice constant a_0 and the Poisson ration ν of the (CsCl)$Co_{0.5}Si$ phase can be obtained by plotting the difference $(a_{\parallel}-a_{\perp})$ as a function of $a_{\parallel}$. The result obtained for films grown with and without a template, and thicknesses ranging from 29 to 96 Å, is shown in Fig. 3. The extrapolation to $a_{\parallel}-a_{\perp}=0$ yields $a_0=(2.69\pm0.01)$ Å, and the slope yields $\nu=0.33$. This is in good agreement with the lattice parameter of 2.68 Å reported by Pirri *et al.*[16] Table I shows the lattice constants of the different iron and cobalt silicides with the CsCl structure, and the corresponding Poisson ratios, determined by XRD measurements.[19–21] For comparison results for $CoSi_2$ with the fluorite structure are also given. For both the iron and cobalt silicides, the lattice constant increases with the metal content. The same Poisson ratios were obtained for all silicides, probably due to the same local bonding of the metal atom inside a cubic Si cage.

Due to the negative misfit $f=(2a_0-a_{Si})/a_{Si}=-0.9\%$, the $Co_{0.5}Si$ layers are under a tensile strain as long as the interfaces remain coherent, i.e., $2a_{\parallel}=a_{Si}$ and $\varepsilon_t>0$. The XRD results show that the films can be grown coherently on

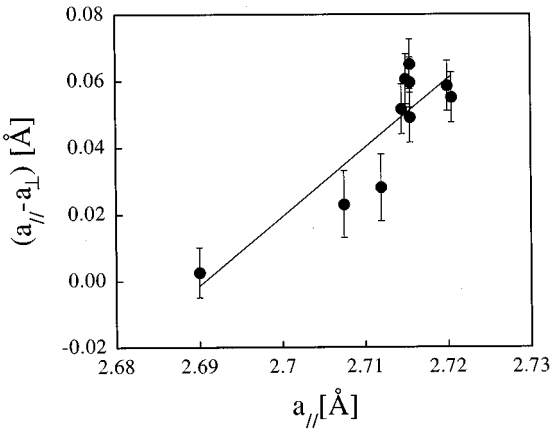

FIG. 3. Difference between the parallel and perpendicular parameters of the $Co_{0.5}Si$ films as a function of the parallel parameters. The extrapolation of the curve at zero and the slope yield $a_0=(2.69\pm0.01)$ Å and $\nu=0.33$, respectively.

Si(111) at RT up to thicknesses ≈100 Å, and the resulting trigonal strain is found to be $\varepsilon_t=2.20\pm0.15\%$. Figure 4 shows the trigonal distortion as a function of the thickness for films of $Co_{0.5}Si$ (filled circles) grown at RT, and $CoSi_2$ annealed to 600 °C (open circles).[25] For both structures, the films were grown onto a preformed template, and on a Si(111) substrate with the same misorientation. For thicknesses above 100 Å, the $Co_{0.5}Si$ films slightly relax the strain by introducing misfit dislocations, without a change of crystal structure.[26] For $CoSi_2$ biaxial strain relaxation sets in at a thickness of $h_c\approx45$ Å.[25] The thick layers are completely relaxed at the growth temperature, and the measured strain is induced by the different thermal expansion of Si and $CoSi_2$, with $\varepsilon_t(\text{thermal})=0.74\%$.[25] Finally, all $Co_{0.5}Si$ films formed without a template exhibited a smaller tensile strain than equally thick ones grown onto a template. In all cases, we found that $\varepsilon_t(T)=1.2\varepsilon_t$, where $\varepsilon_t(T)$ and ε_t denote the trigonal strain for the films grown with and without a template, respectively. This is consistent with the smaller dislocation density observed by TEM in films grown on a template.[13]

IV. ELASTIC PROPERTIES

In order to determine the whole set of elastic constants of films with both structures, Brillouin spectroscopy on surface acoustic waves (SAW's) was used.[27] A surface acoustic wave is a superposition of waves propagating along the surface. The amplitude u_0 along the surface normal is exponentially damped, whereby the wave intrudes only a few micrometers.

All measurements were performed in exact backscattering geometry at room temperature with a wavelength of the Ar^+ laser of $\lambda=514.5$ nm. Films with a thickness h of 100, 270, and 1000 Å were examined. The in-plane component q of the wave vector k_0 of the laser beam was pointing along [110]. The SAW also propagates along this direction. Its velocity depends on the thickness h of the film and $q=2k_0\sin\theta$, where θ is the angle between the incident beam and the surface normal.

With Brillouin spectroscopy the frequency shift $\Delta\omega$ be-

TABLE I. Lattice constants and Poisson ratios determined by XRD measurements of iron and cobalt silicides with the CsCl sructure, and for $CoSi_2$ with the fluorite structure (Ref. 30).

	$Co_{0.5}Si$	CoSi	$Fe_{0.5}Si$	FeSi	$(CaF_2)CoSi_2$
a_0 (Å)	2.69±0.01	2.74±0.02	2.70±0.02	2.77±0.01	5.365
υ	0.33	0.32	0.33	0.33	0.38

tween incident and scattered photons is measured. Using the conservation of energy and momentum, the sound velocity ν_{SAW} of the SAW can be calculated from $\Delta\omega$.

In a bulk material ν_{SAW} depends only on the elastic constants C_{ij} and the mass density ρ_m.[28] For a thin film on a substrate ν_{SAW} is a function of C_{ij} and ρ_m of both the film and the underlying substrate, and furthermore of the product qh. Therefore, by varying the angle θ, and in turn q, the qh dispersion can be measured.[29] In Fig. 5 the measured velocities of all samples are plotted against qh. ν_{SAW} are accurate to within ±2%. Obviously, the thinner the film the larger the influence of the substrate on the velocity of the SAW. For $qh \Rightarrow 0$, ν_{SAW} converges to the value for pure Si (4546 m/s).

In each material an independent set of three exponentially decreasing and increasing waves can be determined from the equation of motion. In the substrate the wave has to be strictly damped, whereas in the film the superposition of waves with both decreasing and increasing amplitudes are allowed. To obtain a unique solution of this nine-dimensional problem several boundary conditions have to be fulfilled. Hence at the *free* surface, all stress components must vanish. Moreover, at the film/substrate interface the continuity of wave amplitude and stress is required. Since the two thicker films were capped with 40 Å of Si, the fit model was extended to a substrate with two thin films on it. This increases the complexity from nine dimensions up to 15. As a further boundary condition the interface between the silicide film and the protecting Si had to be considered.

This elastic continuum model was used to fit the measured ν_{SAW} with C_{11}, C_{12}, and C_{44} of the silicide as parameter. The elastic constants of the Si substrate and the protecting Si layer were kept constant together with the densities. The fits are shown in Fig. 5, and the elastic constants resulting from the fit procedure are given in Table II. The curves are not drawn in a continuous fashion because the Si cap is absent on the 100-Å sample. The fit was, however, performed for the complete set of measured velocities for both crystal structures.

For the CaF_2 structure C_{11} and C_{12} agree with previously published values,[30–32] while for C_{44} the difference is quite large. This can be explained by the weak dependence of the model function on C_{44} in the (111) plane, lowering the accuracy of this fitting parameter. For the CsCl defect structure no elastic measurements were published before, to our knowledge.

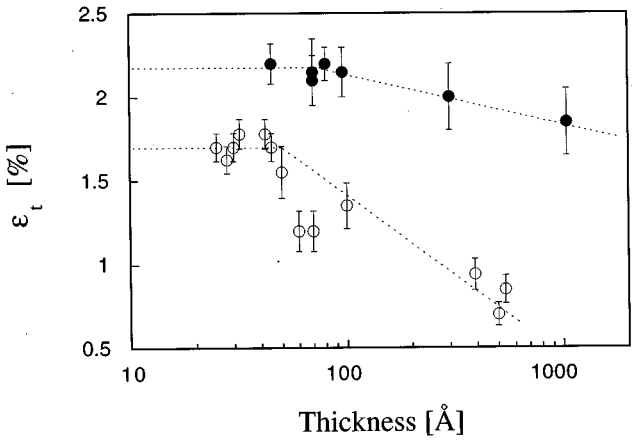

FIG. 4. Trigonal distortion of $(CaF_2)CoSi_2$ films (open circles) and $(CsCl)Co_{0.5}Si$ films grown at RT (filled circles) as a function of the film thickness. Up to ≈100 Å, the $Co_{0.5}Si$ films are coherent, and, for thicker thicknesses, the strain starts to release continuously. For the $CoSi_2$ films the critical thickness for biaxial strain relaxation is ≈45 Å.

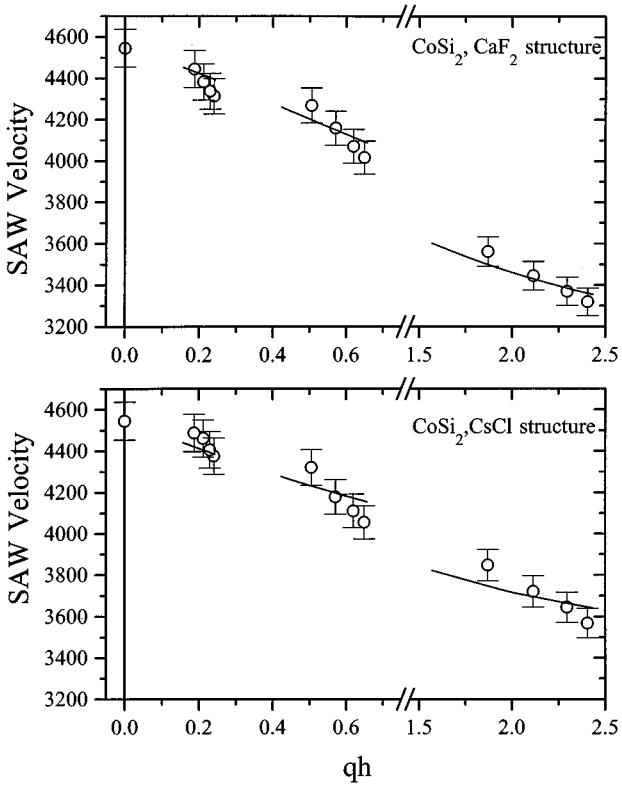

FIG. 5. qh dispersion of the surface acoustic wave measured on $CoSi_2$ with the CaF_2 (upper graph) and CsCl (lower graph) structures on Si(111). The thicknesses of the film are 100, 270, and 1000 Å (corresponding to qh of 0.18–0.24, 0.50–0.65, and 1.87–2.40). The direction of propagation is [110]. The error bars of the velocities are 2%. The horizontal error bars are due to the uncertainty of the film thickness of about 10%. The continuous curve segments are calculated from the fitted elastic constants (Table II). They are segmented because of a 40-Å-thick protecting Si film which is lacking on the thinnest sample.

TABLE II. Elastic constants of both structures of $CoSi_2$ obtained by Brillouin spectroscopy, literature, and calculations (see also text). ρ_m is the mass density, B the bulk modulus, υ the Poisson's ratio, and η the anisotropy.

Structure of $CoSi_2$	C_{11} (GPa)	C_{12} (GPa)	C_{44} (GPa)	ρ_m (kg m^{-3})	B (GPa)	υ	η	Reference
CaF_2	227±10	145±10	112±20	4941	172±10	0.39±0.04	2.75±1.15	this work
CaF_2	228	140	83		169	0.38	1.89	28
CaF_2	240	161	74		187	0.40	1.87	29
CaF_2	222	140	68		167	0.39	1.66	30
CsCl	260±10	128±10	64±20	4773	172±10	0.33±0.04	0.96±0.45	this work
CsCl (Voigt's average)	258±26	129±18	64±28		172±20	0.33±0.08	0.99±0.77	this work

In order to obtain a better picture of the differences in the elastic behavior of the two structures, several elastic properties were calculated from the elastic constants. The bulk modulus, defined by

$$B=\tfrac{1}{3}[C_{11}+2C_{12}], \tag{4}$$

is the same for both structures according to Table II.

The Poisson ratio is the negative of the perpendicular strain over the longitudinal one, when uniaxial stress is applied. If the longitudinal axis corresponds to one of the main crystallographic directions [(100), (010), or (001)], it can be written as

$$\upsilon=\frac{C_{12}}{C_{11}+C_{12}}. \tag{5}$$

It is usually located in the range 0.20–0.40, and for $\upsilon=0.5$ the volume would be exactly preserved, a situation that never occurs in real materials. However from Table II we see that fluorite $CoSi_2$ appears to be more deformable than the defected structure.

The anisotropy shows the largest difference. For an isotropic material the transverse velocity of an acoustic wave, propagating along the ⟨110⟩ direction, does not depend on its polarization (i.e., the sound velocity $\nu_{T1}=\sqrt{C_{44}/\rho_m}$ for displacement along [001] is equal to $\nu_{T2}=\sqrt{(C_{11}-C_{12})/2\rho_m}$ for displacement along [110]). The anisotropy η is defined by the squared ratio of both transverse mode velocities:

$$\eta=\left(\frac{\nu_{T1}}{\nu_{T2}}\right)^2=\frac{2C_{44}}{C_{11}-C_{12}}. \tag{6}$$

According to Table II the anisotropy of the CaF_2 structure exceeds unity, whereas the CsCl structure behaves isotropically. The isotropy of the CsCl phase is confirmed from measurements of the angular dispersion[28] in the (111) plane (variation of ν_{SAW} as a function of the in-plane azimuth). The anisotropy parameters are probably so different because the two structures differ in the location of the Co atoms, a feature which affects the directional dependence of the elastic constants. In the CaF_2 structure, Co atoms are placed regularly, whereas in the defect CsCl structure they are located randomly over the whole lattice. The latter can be considered as an average of the first one. This can be checked by applying *Voigt's average* to the elastic constants of single-crystalline $(CaF_2)CoSi_2$, where upon those of the polycrystalline material are obtained. A polycrystalline phase always behaves isotropically, since all crystallographic directions are equivalent. For the averaging, our inaccurate value for C_{44} of 112 GPa was replaced by an average literature value of 80 GPa. Then the calculated values of the CsCl structure fit the measured ones very nicely.

V. THERMAL STABILITY

By annealing the $Co_{0.5}Si$ films, one can induce a phase transition to the stable fluorite phase of $CoSi_2$, which requires ordering of the Co atoms. In order to determine the amount of transformed material, we analyzed the ratio of the integrated intensities for two asymmetrical x-ray reflections. We have measured (I_{440}/I_{331}) as a function of the annealing temperature for two films of different thickness grown on a 10-Å-thick $CoSi_2$ template. Figure 6 shows the experimental ratios for $h=45$ Å (filled circles) and $h=80$ Å (open circles). The corresponding theoretical ratio[24] for the CaF_2 structure of $CoSi_2$ yields 1.5.

The result shows the same behavior for both films, with a gradual transition to the stable $CoSi_2$ phase: (i) Up to 200 °C, the films have almost entirely a CsCl structure. (ii) Around 250 °C, approximately half of the films are transformed. (iii)

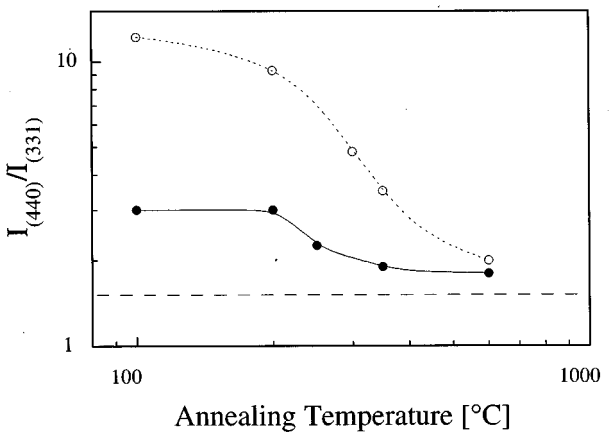

FIG. 6. Experimental ratio of the integrated Bragg peak intensities (I_{440}/I_{331}) as a function of the annealing temperature, of two films grown onto a template with thicknesses of 45 (filled circles) and 80 Å (open circles), respectively. The dashed line shows the theoretical ratio for the fluorite structure of $CoSi_2$.

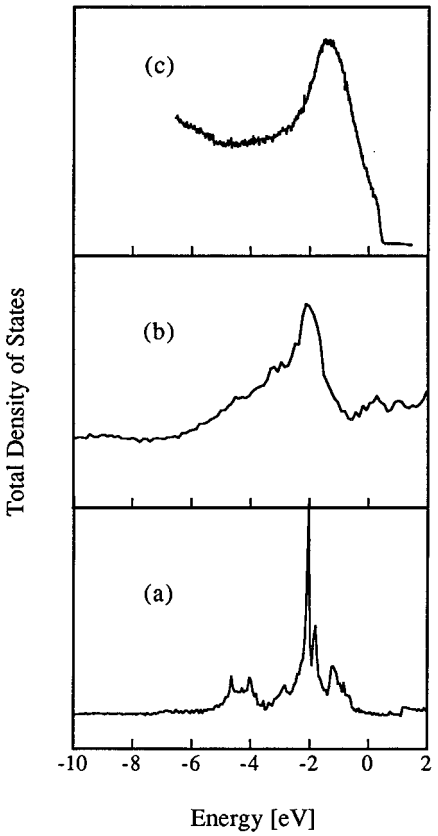

FIG. 7. Electronic density of states for $CoSi_2$ with the CaF_2 (a) and CsCl (b) structures. (c) Photoemission measurements on a 45-Å-thick (CsCl)$Co_{0.5}Si$. The Fermi levels are aligned at zero energy.

Above 350 °C, the films consist primarily of a $CoSi_2$ phase with a CaF_2 structure. A higher temperature for the transition (≈500 °C) has been found by photoemission measurements.[16] The XRD investigations alone do not reveal any difference between films formed with and without a template, once they have been annealed at high temperature. Nevertheless, it has been shown that for $CoSi_2$ films grown onto a template, grains with the defect-CsCl structure are sometimes present even after anneals to 600 °C.[17]

VI. TIGHT-BINDING RESULTS

In order to understand the easy occurrence and the remarkable stability of CsCl-defected grains, we performed total-energy calculations and molecular-dynamics simulations with a semiempirical interatomic potential used successfully for the interpretation of the stability hierarchy in $FeSi_2$,[33] FeSi, and CoSi (Ref. 19) epitaxial phases. The potential is obtained by partitioning the total energy into an attractive part E_{bs}, originating from a summation over occupied tight-binding states $\varepsilon_{n,k}$ (n is the band index and k the wave vector), and a repulsive contribution $E_{\rm rep}$ which is generated by summing a short-range, two-body potential $\Phi(r_{ij})$ over the relevant shell of neighbors (j),

$$E = E_{bs} + E_{\rm rep} = \sum_{nk} \varepsilon_{nk} + \sum_{i<j} \Phi(r_{ij}). \qquad (7)$$

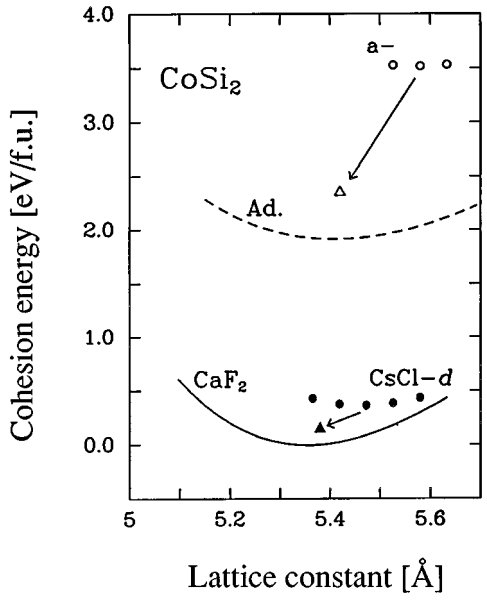

FIG. 8. Total-energy curves with fluorite lattice constant for the $CoSi_2$ phases. From the bottom to the top: bulk stable fluorite structure (solid line), defected CsCl phase (filled circles), and adamantane structure (dashed line).

E_{bs} is negative and takes into account the covalent attraction provided by the orbitals hybridization and overlap, whereas $E_{\rm rep}$ is positive and phenomenologically represents the quantum-mechanical interaction between occupied orbitals. More details about our potential can be found in Refs. 33 and 34.

Figures 7(a) and 7(b) show the electronic density of states for fluorite and defected $CoSi_2$, respectively, as calculated by our tight-binding parameters. We see that the former displays three main features, whereas the latter shows only one broad structure, with the Fermi level located on a small peak at higher energy, as it was the case for CsCl-defected FeSi.[33] This picture nicely corresponds to the photoemission data measured on a 45-Å-thick $Co_{0.5}Si$ film, which agree well with the measured ones by Pirri *et al.*,[16] and they are also reported in Fig. 7(c) for comparison. If the main peak in both structures is aligned to the one of our calculated density of states (DOS), we see that the quantitative agreement is good for all the features reported above and our DOS for the defected phase, as averaged over eight random configurations, can be considered as a reliable picture of the electronic states.

In Fig. 8 we show the total-energy curves as calculated by our tight-binding scheme. Starting from the bottom we correctly find the bulk stable fluorite structure (solid line) and the defected CsCl phase (black dots), where 50% of the cobalt sites are randomly occupied (we display an average over 12 configurations in a 96-atom cubic simulation cell). Sensibly higher in energy is located the adamantane phase (dashed line), which corresponds to an interchange between Si and Co sites, resulting in a diamond crystal with metallic interstitials in a tetrahedral configuration. Actually the latter structure can also be interpreted as a bcc network where the ordered distribution of Si, Co, and empty sites is different from fluorite. Even the CsCl-defected structure fits this

scheme, but for the random occupation of the Co sites. It is therefore easy to extrapolate a model for the amorphous phase where each bcc site is randomly occupied either by Si, Co, or voids, retaining the $CoSi_2$ stoichiometry. The total-energy results corresponding to an average over eight random configurations in the 96-atom cubic simulation cell are at the top of the figure (open circles). The latter structure and the CsCl defected one do, however, display site disorder in a perfectly cubic bcc network. A decrease in energy could thus be expected by allowing lattice relaxation. Therefore we performed molecular-dynamics simulations with our interatomic potential for one configuration in each of the two cases, starting from the volume corresponding to the lowest energy. The lattice relaxation is performed by a 96-atom simulation cell with variable shape and size, at zero pressure and 100 K. The triangles in Fig. 8 indicate the corresponding decrease in energy and volume per atom that we obtained. This is probably just a rough estimate of the relaxation process. It does, however, point out that the stability hierarchy is unchanged, and that the main issue is the large energy gap existing between the phases with the cobalt atom positioned at the center of cubic silicon cages (fluorite and CsCl defected) and the one where this local configuration is different (adamantane and amorphous). In Ref. 34 we already analyzed the origin of such a gap for the unrelaxed configurations by inspecting the changes in E_{bs} and $E_{\rm rep}$. We showed that the stability of fluorite and defected structures comes essentially from the cohesive action of the covalent bond, which in turn is provided by the fact that the cubic cage of silicon atoms around the cobalt maximizes the overlap between the sp^3 hybrids of the former and the $d_{\alpha\beta}$ hybrids of the latter. The slight increase of the CsCl-defected energy mainly comes from some second neighbor repulsive contribution between Co-Co pairs.

By considering the contribution of configurational disorder to the entropic part of the free energy for the unrelaxed networks, the CsCl-defected and amorphous data do not change their energy positions appreciably, since at room temperature $-ST$ is -0.034 and -0.104 eV/f.u., respectively. The vibrational density of states at low frequency is not expected to change appreciably from one phase to the other (see, for example, the elastic constants in the preceding sections), so that neither the vibrational contribution to the entropic part of the free energy should change the picture of Fig. 8. Therefore we conclude that a large thermodynamic driving force is present in the transformation from amorphous to fluorite or CsCl-defected phases, whereas only a feeble one is expected between the latter two. This is confirmed by very preliminary Metropolis Monte Carlo simulations with our potential. They indicate that, by disregarding the kinetic barrier effects through first-neighbor interchanges in the bcc network, the evolution of amorphous to CsCl-defected phase is readily obtained with prompt formation of cubic silicon cages. No evolution to the fluorite structure is observed within our limited simulation times and configurations.

We are convinced that kinetic effects drive the transformation from CsCl-defected to fluorite phases, and that the energy barrier provided by the cubic cage of silicon atoms around the cobalts is the limiting factor for the short-path diffusion to the ordered configuration. To check this point we performed several molecular dynamics simulations, at temperatures between 800 and 1200 K, and simulation times as long as several picoseconds, with different starting configurations in a 96-atom supercell:

(i) No relevant atomic displacements (but for the thermal disorder) were observed in the case of ''perfect'' CsCl-defected configuration with all Si cubic sites occupied.

(ii) In the case of one Si vacancy we observed relaxation of Co or Si neighboring atoms, but no indirect hopping of any metal from one site to another through this ''corner vacancy.''

(iii) By substituting two (001) atomic layers over eight in the simulation cell (one Co and one Si, respectively) with two Si layers arranged in a diamond network, we observed a strong tendency of the cubic Si network to reconstruct (leaving a void layer behind) and the Co atoms to jump from one site to another with fewer Co second neighbors, as is the case for a local fluorite arrangement. The important fact is that the hopping always occurs throughout the square faces of the cubic Si cage, by taking profit of their relaxed arrangement nearby the reconstructed (or still reconstructing) Si bilayer.

Therefore we conclude that Co diffusion seems not to occur through Si vacancies, but straightforwardly from one metal site to another, and that it is strongly activated by Si network distortions, as it might occur at internal extended defects or at silicon interfaces. These predictions are in agreement with recent experiments of Co and Si self (isotope) diffusion in fluorite $CoSi_2$ at temperatures above 700 K, showing that in both cases grain boundary diffusion is several orders of magnitude (10^6) faster than lattice diffusion, that in any case the activation energies are quite high (2.5–3.2 eV), and that diffusion coefficients are unaffected by stoichiometry variations giving rise to point defects.[35]

VII. ELECTRICAL PROPERTIES

The dependence of the resistivity on temperature, $\rho(T)$, of films grown with and without a template was measured between 4.2 and 300 K. $Co_{0.5}Si$ films with the defect-CsCl structure exhibit a high residual resistivity ρ_0(4.2 K) between 95 and 155 $\mu\Omega$ cm, for all film thicknesses. No dependence of ρ_0 on film thickness was found, in contrast to $CoSi_2$.[1,36]

For films with ρ_0(4.2 K) up to 115 $\mu\Omega$ cm, Matthiessen's rule for normal metals is always obeyed. Thus the resistivity can be expressed as $\rho(T)=\rho_0+\rho_{\rm ph}(T)$, where ρ_0 is the residual resistivity which is due to carrier scattering by structural defects, impurities, etc., and $\rho_{\rm ph}(T)$ is the contribution of electron-phonon scattering. For the films with ρ_0 above 123 $\mu\Omega$ cm, the influence of the electron-phonon scattering becomes negligible. We attribute the high residual resistivity to the large number of Co vacancies in the defected-CsCl structure.

For the two kinds of films grown at low temperature on the same substrate, the one with a template has a *smaller* resistivity, which can be understood by the fact that the template contributes to the conductivity. Figure 9(a) displays $\rho(T)$ for a 60- (70-) Å-thick film on the substrate region without (with) a template. It was annealed to 350 °C for 2 min. After annealing at higher temperatures the behavior is reversed, and the side with the template exhibits a *larger* $\rho(T)$. This can be seen in Figs. 9(b) and 9(c), corresponding to $T_A=600$ and 650 °C, respectively. For $T_A=650$ °C, the

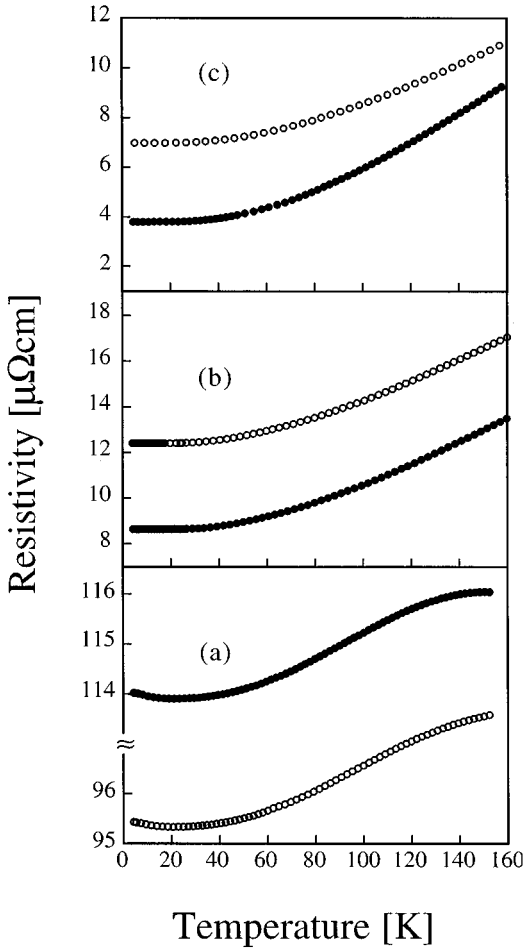

FIG. 9. Resistivity as a function of the temperature for two films of 60-Å-thick grown on the same substrate, with the use of a 10-Å-thick template (open circles), and without template (filled circles). From the top to the bottom: after an anneal to 350 °C for 2 min (a), 600 °C for 60 min (b), and 650 °C for 30 min (c).

film without a template has a resistivity close to that of bulk material, indicating good crystal quality. On the other hand, ρ_0 of the thicker film on the template is nearly twice as large. We attribute the poorer electrical properties of $CoSi_2$ films grown onto a template to an incomplete ordering of the Co atoms, or, equivalently, to the presence of $Co_{0.5}Si$ grains with a defected CsCl structure.

At 4.2 K the Hall voltage varied linearly with the magnetic field up to 5 T for all $(CsCl)Co_{0.5}Si$ films. As for $(CaF_2)CoSi_2$,[37,38] holes were found to be the dominant carrier species. The hole densities deduced from a one-band model are in the range of $(1.6\pm0.20)\times10^{22}$ cm^{-3} independent of the film thickness. For $Co_{0.5}Si$ films with templates, the density is generally 15% larger. After post-growth annealing, the $CoSi_2$ films grown without templates show a typical value of $(2.2\pm0.20)\times10^{22}$ cm^{-3} very close to the carrier concentration for bulk $CoSi_2$.[37] By contrast, the density of films grown onto a template becomes smaller, i.e., $n_h=(1.3\pm0.10)\times10^{22}$ cm^{-3}. Thus the different degree of ordering of the two kinds of films reflects itself very clearly in their electrical properties, even in cases when the two can no longer de distinguished by structure sensitive experimental techniques.

VIII. CONCLUSION

We have shown that films of $CoSi_2$ grown by codeposition at low substrate temperature, with and without a template, crystallize with the CsCl-defected structure, with a lattice parameter $a_0=(2.69\pm0.01)$ Å. The CsCl-defected structure is quite similar to the fluorite arrangement (formation energy, lattice parameter, elastic constants), since they both satisfy the structural requirement of Co atoms inside a cubic Si cage, which in turn is dictated by suitable orbital overlap.

Consequently, the transition from CsCl-defected to fluorite structures is mainly governed by kinetic factors associated with the reordering of the Co distribution on the metal sites, by hopping from occupied sites to empty ones. Presumably this happens by a straightforward jump through the square faces of the cubic silicon cage, which involves a high activation barrier and a low diffusion coefficient. The presence of extended defects and of Si cage distortions can, however, greatly enhance the rate of successful jumps.

Growth onto a fluorite template provides higher quality films, in particular a lower density of dislocations. The slower kinetics of these films for the final transformation from CsCl-defected to fluorite structure explains their poorer electrical properties. Moreover, it is very probable that the persistence of CsCl grains after annealing to 600 °C results from the termination of fast diffusion paths related to extended defects, and to the onset of inefficient lattice diffusion of Co atoms in a perfect Si network.

ACKNOWLEDGMENT

Financial support from the Swiss National Science Foundation is gratefully acknowledged.

[1] H. von Känel, J. Henz, M. Ospelt, J. Hugi, E. Müller, N. Onda, and A. Gruhle, Thin Solid Films **184**, 295 (1990).
[2] J. C. Hensel, A. F. J. Levi, R. T. Tung, and J. M. Gibson, Appl. Phys. Lett. **49**, 522 (1986).
[3] E. Rosencher, P. A. Badoz, C. H. Pfister, F. Arnaud d'Avitaya, G. Vincent, and S. Delage, Appl. Phys. Lett. **49**, 217 (1986).
[4] L. Pahun, Y. Campidelli, F. Arnaud d'Avitaya, and P. A. Badoz, Appl. Phys. Lett. **60**, 1166 (1992).
[5] C. Schwarz, U. Schärer, P. Sutter, R. Stalder, N. Onda, and H. von Känel, J. Cryst. Growth **127**, 659 (1993).
[6] R. T. Tung, J. M. Gibson, and J. M. Poate, Appl. Phys. Lett. **42**, 888 (1983).
[7] J. C. Bean and J. M. Poate, Appl. Phys. Lett. **37**, 643 (1980).
[8] R. T. Tung, A. F. J. Levi, and J. M. Gibson, Appl. Phys. Lett. **48**, 635 (1986).
[9] A. E. M. J. Fischer, W. F. J. Slijkerman, K. Nakagawa, R. J. Smith, J. F. van der Veen, and C. W. T. Bulle-Lieuwma, J. Appl. Phys. **64**, 3005 (1988).

[10] J. Henz, H. von Känel, M. Ospelt, and P. Wachter, Surf. Sci. **189/190**, 1055 (1987).
[11] J. Henz, M. Ospelt, and H. von Känel, Solid State Commun. **63**, 445 (1987).
[12] T. L. Lin, R. W. Fathauer, P. J. Grunthaner, and C. d'Anterroches, Appl. Phys. Lett. **52**, 804 (1988).
[13] R. T. Tung and F. Schrey, Appl. Phys. Lett. **54**, 852 (1989).
[14] H. von Känel, Mat. Sci. Rep. **8**, 193 (1992).
[15] S. L. Zhang, J. Cardenas, F. M. d'Heurle, B. G. Svensson, and C. S. Petersson, Appl. Phys. Lett. **66**, 58 (1995).
[16] C. Pirri, S. Hong, M. H. Tuilier, P. Wetzel, and G. Gewinner, Phys. Rev. B **53**, 1368 (1996).
[17] H. von Känel, E. Müller, S. Goncalves-Conto, C. Schwarz, and N. Onda, Appl. Surf. Sci. (to be published).
[18] H. von Känel, K. A. Mäder, E. Müller, N. Onda, and H. Sirringhaus, Phys. Rev. B **45**, 13 807 (1992).
[19] H. von Känel, C. Schwarz, S. Goncalves-Conto, E. Müller, L. Miglio, F. Tavazza, and G. Malegori, Phys. Rev. Lett. **74**, 1163 (1995).
[20] N. Onda, H. Sirringhaus, S. Goncalves-Conto, C. Schwarz, S. Zehnder, and H. von Känel, Appl. Surf. Sci. **73**, 124 (1993).
[21] N. Onda, H. Sirringhaus, S. Goncalves-Conto, C. Schwarz, E. Müller, and H. von Känel, in *Evolution of Surface and Thin Film Microstructure*, edited by H. A. Atwater, E. Chason, M. Graćow, and M. Lagally, MRS Symposia Proceedings No. 280 (Materials Research Society, Pittsburgh, 1993), p. 581.
[22] J. Hornstra and W. J. Bartels, J. Cryst. Growth **44**, 513 (1978).
[23] B. E. Warren, *X-Ray Diffraction* (Addison-Wesley, Reading, MA, 1969).
[24] B. D. Cullity, *Elements of X-Ray Diffraction*, 2nd ed. (Addison-Wesley, Reading, MA, 1978).
[25] C. Schwarz, N. Onda, S. Goncalves-Conto, H. Sirringhaus, and H. von Känel, J. Appl. Phys. **76**, 7256 (1994).
[26] S. Goncalves-Conto, E. Müller, K. Schmidt, and H. von Känel, in *Silicide Thin Films—Fabrication, Properties and Applications*, edited by R. T. Tung, K. Mack, P. W. Pellegrini, and L. H. Allen, MRS Symposia Proceedings No. 402 (Materials Research Society, Pittsburgh, 1996), p. 493.
[27] M. W. Elmiger, J. Henz, H. von Känel, M. Ospelt, and P. Wachter, Surf. Interf. Anal. **14**, 18 (1989).
[28] G. W. Farnell, *Physical Acoustics* (Mason, New York, 1970), Vol. VI, p. 109.
[29] G. W. Farnell, *Physical Acoustics* (Mason, New York, 1972), Vol. IX, p. 35.
[30] G. Guénin, M. Ignat, and O. Thomas, J. Appl. Phys. **68**, 6515 (1990).
[31] L. Weiss, A. Y. Rumyantsec, and A. S. Ivanov, Phys. Status Solidi B **128**, K111 (1985).
[32] M. Mendik, Ph.D. Thesis, ETH Zürich, 1993.
[33] Leo Miglio, Francesca Tavazza, and Giovanna Malegori, Appl. Phys. Lett. **67**, 2293 (1995).
[34] Leo Miglio and Francesca Tavazza, in *Silicide Thin Films—Fabrication, Properties and Applications* (Ref. 26).
[35] T. Barge, P. Gas, and F. M. d'Heurle, J. Mater. Res. **10**, 1134 (1995).
[36] J. M. Phillips, J. L. Bastone, J. C. Hensel, and M. Cerullo, Appl. Phys. Lett. **51**, 1895 (1987).
[37] J. C. Hensel, in *Thin Films—Interfaces and Phenomena*, edited by R. J. Nemanich, MRS Symposia Proceedings No. 54 (Materials Research Society, Pittsburgh, 1986), p. 499.
[38] K. Radermacher, D. Monroe, A. E. White, K. T. Short, and R. Jebasinski, Phys. Rev. B **48**, 8002 (1993).